# 2D Particle-in-Cell Channel Simulation of the Narrow Channel Hall Thruster

**IEPC-2019-642**

*Presented at the 36th International Electric Propulsion Conference*
*University of Vienna, Austria*
*September 15-20, 2019*

Igal Kronhaus* and Omri Hamo†
*Technion - Israel Institute of Technology, Haifa 3200003, Israel*

**Abstract: A miniature Hall thruster was developed in the Aerospace Plasma Laboratory (APL), Technion, designed to operate at low voltages and mass flow rates. The so called narrow channel Hall thruster (NCHT) represents a compromise between exhaust velocity and operating power and is of unconventional construction. The thruster proportions were selected to maintain sufficient gas density in low mass flow rates, resulting in a very narrow and short channel compared to classical design. At a discharge power of 20 W a thrust of 1 mN is generated with anode efficiency of 6.6 %. The thruster design was analyzed using a 2D particle-in-cell simulation. For a mass flow rate 0.38 mg/s, good agreement is obtained between the simulation and experimental parametric results. The simulation enables to study the spatial variation of plasma parameters inside the channel. It is shown that the discharge is maintained by an increased axial electron current that contributes about half of the discharge current.**

## Nomenclature

| | |
|---|---|
| $B_r$ | = radial magnetic field strength |
| $d_m$ | = channel diameter |
| $dt$ | = electron time step |
| $E_i$ | = ion energy |
| $e$ | = unit charge |
| $H$ | = grid cell size |
| $h$ | = channel width |
| $I_d$ | = discharge current |
| $I_{i,ex}$ | = Ion current at the exit plane |
| $M$ | = xenon mass |
| $m_e$ | = electron mass |
| $n$ | = number density |
| $T$ | = thrust |
| $U_d$ | = Discharge voltage |
| $v_e$ | = electron velocity |
| $w_i$ | = ionization rate |
| $\sigma_i$ | = ionization cross section |
| $\Omega_e$ | = Hall parameter |

*Professor, Faculty of Aerospace Engineering, kronhaus@technion.ac.il.
†Ph.D. candidate, Faculty of Aerospace Engineering.

# I. Introduction

Hall thrusters (HT) were historically designed to operate at power levels above 300 W.[1] Scaling the conventional SPT like design to lower operating power has proven to be difficult. Reports in the literature,[2] indicate an electrical efficiency drop to 10 - 30 % at power levels below 100 W. The poor performance of low power regimes is mostly attributed to low propellant utilization.[3] No reports are given of successful operation of conventional HTs below 50 W.

HTs are classified as electrostatic thrusters, characterized by the fact that the exhaust velocity is proportional to the square root of the discharge voltage. Therefore, previous attempts at power reduction focused on keeping the original discharge voltage level, maintaining the specific impulse of the thruster, while sharply lowering the discharge current. A lower current implies lower propellant mass flow rate; the decreased mass flow rate results in an increased ionization mean free path length and leads to lower probability of propellant ionization.

Methods of improving propellant utilization can be divided into two categories: 1) channel extension; 2) increasing the initial residual plasma density. The former techniques have shown to provide only limited gains due to an increase in wall recombination rate.[4] For the later techniques a typical approach is to use a double stage thruster configuration, where the plasma is generated by a specialized stage that feeds a conventional accelerator stage. Several thruster designs of this type were previously described in the literature.[5] Although some double-stage designs show promise, they involve added complexity both to the thruster design and discharge physics.

Recently, a concept of a very low power Hall thruster was developed at the Aerospace Plasma Laboratory (APL), Technion, the so called narrow channel Hall thruster (NCHT). The NCHT has shown excellent thrust to power capability $\approx 50$ $\mu$N/W operating at power levels as low as 15 W.[6] With a thrust level of 1 mN at 20 W and potential lifetime of more than 1000 h the NCHT is well suited to serve as a main propulsion system for large nanosatellites. This paper provides simulation results of the discharge in the NCHT channel. The NCHT is described in section II. The particle-in-cell (PIC) model of the NCHT is described in section III, and the simulation results are analyzed and discussed in section IV.

# II. Narrow Channel Hall Thruster

Instead of following conventional dimensional scaling that keeps the ratio of channel width to mid channel of $h/d_m \approx 1/6$ (as in the venerable SPT-100), the NCHT utilizes a narrow channel with a ratio of $h/d_m \approx 1/30$. A schematic of the NCHT is shown in Fig. 1. The channel is formed between two concentric metal walls that serve as the magnetic poles. A single magnetic coil, placed far away and inline to the channel, energizes the poles. A metal gas distributor functions as the anode whereas the metal walls are under cathode potential.

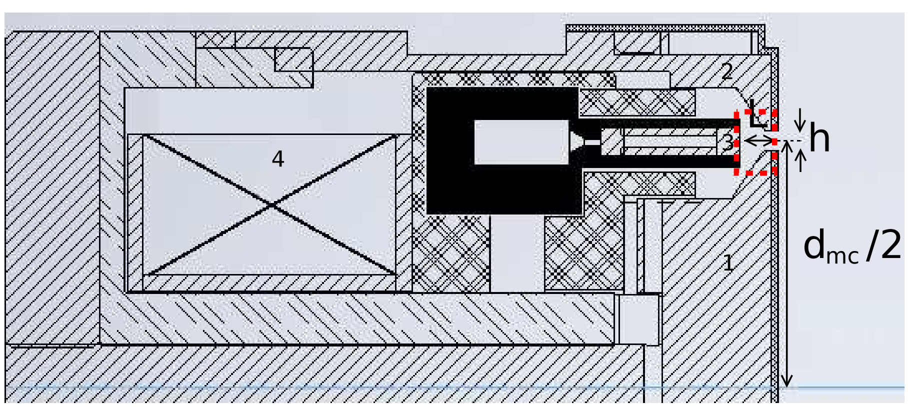


**Figure 1. Schematic cross sectional view of the NCHT experimental model. (1) Inner pole; (2) Outer pole; (3) Gas distributor/Anode; (4) Coil. Both poles under cathode potential. The channel region is marked by a rectangle. An external cathode is placed outside the thruster (not shown).**

The NCHT narrow channel, only 1 mm wide, allows increasing the gas density in the region of high magnetic induction improving the ionization rate. The channel has a variable width, decreasing in size downstream towards the exit. This shape provides both sharp tips at the poles, that allow generation of strong magnetic induction near the exit, as well as thicker wall upstream to enable higher resistance to sputtering and wall erosion. A photograph of the experimental NCHT model in operation is shown in Fig. 2.

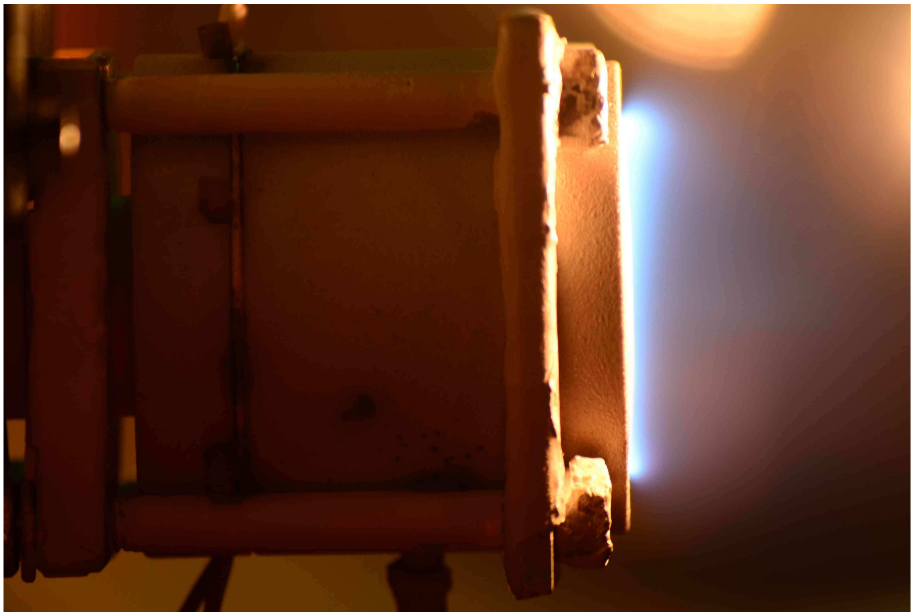

**Figure 2. A photograph of a 3 cm prototype NCHT during operation. The plume is clearly visible near the narrow channel exit.**

## III. Particle-In-Cell Numerical Model

Numerical modeling of the NCHT discharge is performed using XOOPIC-APL,[7] a fully kinetic PIC simulation. XOOPIC-APL is based on the general purpose 2D3V PIC code XOOPIC.[8] XOOPIC-APL utilizes a rectilinear computational grid with an axisymmetric coordinate system. All field quantities are calculated on the grid and assumed to be uniform in the azimuthal direction. Macro-particle velocity is tracked in all three dimensions. The original program was modified to properly model the Hall thruster physics. The code includes the addition of gas dynamics, more advanced particle-boundary interactions and post-processing capabilities. The multiprocessor variant of the program was also refined to the specifics of the model and a parallel Poisson solver was added. The program uses the Monte Carlo collisions (MCC) model for simulating electronneutral collisions.

There are three macro-particle species in the simulation: electrons $e^-$, xenon neutrals Xe, and single charged xenon ions $Xe^+$. Only collisions between electrons and xenon neutrals are modeled, these include: elastic, excitation, and single ionization. Excited atoms and ions are assumed to radiate and immediately return to the ground state.

Xenon neutrals and ions are accommodated on the walls and are emitted back as xenon neutrals. A half-Maxwellian distribution at the wall temperature of 600 K was used for heavy particle emission from the wall, i.e. the emitted particle axial velocity is Maxwellian but restricted to a solid angle of $2\pi$ normal to the wall. The temperature was selected according to measured values of the NCHT experimental model during operation. On the other hand, electrons are absorbed by the walls and boundaries, and therefore are effectively removed from the simulation.

A dynamic alternating direction implicit (ADI) Poisson solver is used to solve the electric field self consistently from the charge density. As shown in Fig. 3, Dirichlet boundary conditions are imposed on all the walls: the left boundary is under anode potential whereas the rest of the surfaces are under cathode potential. The magnetic field was computed using the program FEMM.[9] Calculated and measured radial magnetic field strength in the thruster mid channel are presented in Fig. 4.

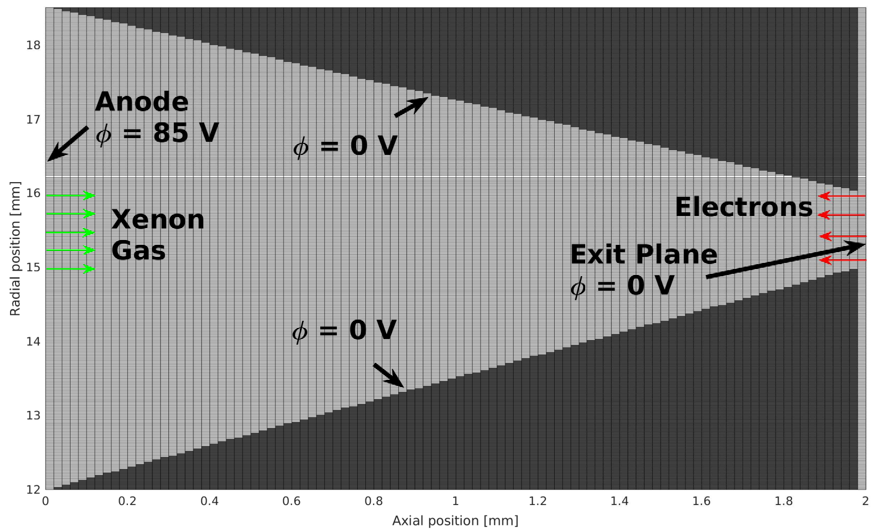


**Figure 3. NCHT channel model computational domain, including boundary conditions and particle emitters.**

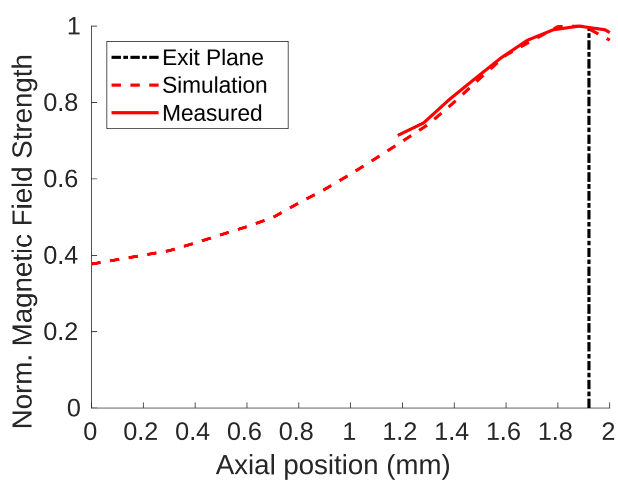


**Figure 4. NCHT radial magnetic-field-strength along the channel length. Both computed and experimentally measured distribution along mid channel are shown.**

To achieve reliable results we follow standard PIC simulation practices[10,11] where each grid cell volume $H^3$ is smaller than Debye sphere and the electron time step $dt$ is chosen according to the ratio $\omega_p dt \approx 0.3$, where $\omega_p$ is the electron plasma frequency. The ratio between the physical particles and the macro-particles $NP2C$ was determined so that the number of macro-particles in each cell is greater than 100. This number is sufficiently large to guaranty that artificial enhancement of the collisional process due to grid scattering is negligible compared to classical transport.[11] The numerical parameters chosen are summarized in Table 1.

**Table 1. Simulation parameters**

| $H_z$, mm | $H_r$, mm | $dt$, s | $N_z$ | $N_r$ | $NP2C$ | $N_c$ |
|---|---|---|---|---|---|---|
| 2 | 6.5 | $5 \times 10^{-12}$ | 100 | 400 | $1.2 \times 10^5$ | $2 \times 10^6$ |

The simulation uses correct physical values for the vacuum permittivity constant as well as species mass and charge. No artificial geometry or dimensional scaling is used. In order to reduce the computational time heavy species are subcycled, i.e., advanced every 50 electron time steps for ions and 500 electron time steps for neutrals.

Although the NCHT channel is relatively small compared to a classical HT a fully kinetic PIC simulation still poses a significant computational demand, and a high performance parallel computing scheme is preferable to obtain results in a reasonable time. XOOPIC-APL has a built-in MPI parallelization capability based on domain decomposition,[7] however, in this work we have chosen a different approach at parallelization using the OpenMP shared-memory architecture.[12]

The modification included the mapping of the code flow and resource allocation using a profiling software.[13] This allowed to identify several parts of the code with parallelization potential, i.e. responsible for a significant part of the run time and include calculations which are independent from each other. In XOOPIC-APL the relevant parts of the code were the particle pusher, the electrostatic field solver, the summation of particle data to the grid points as well as data handling for diagnostics. The result is a speed up factor of 300 % with 6 cores relative to the serial one.

As shown in Fig. 3, the simulation domain includes two types of particle emitters: 1) An electron emitter simulating the cathode-neutralizer, located on the right boundary; 2) A xenon emitter simulating the anode/gas distributor, located left boundary. Electrons are introduced according to a half-Maxwellian distribution at a temperature of 4 eV. At the start of the simulation electrons are emitted from this boundary at a constant current of 0.1 A. Once the discharge is ignited and the ion current on the exit plane boundary exceeds 0.1 A the electron emission is regulated automatically to maintain quasi-neutrality near its surface.[14] We note that no artificial conductivity was introduced in the simulation. Xenon particles are emitted at a half-Maxwellian distribution at a temperature of 0.05 eV; the xenon macro-particles emission rate is predetermined using a fixed mass flow rate.

## IV. Simulation Results

### A. Thruster parametric results

As described in section III, PIC simulations were performed using dimensions and geometry, magnetic field configuration, and input parameters of the NCHT prototype channel. Several cases are studied varying the anode voltage $U_d$, mass flow rate$\dot{m}$ and magnetic coil current $I_{coil}$. In each case, the simulation is initiated by introduction of xenon neutrals and is propagated until a steady-state distribution of gas is established in the channel. Then, electrons are introduced. The plasma simulation is allowed to advance until a steady state is obtained, typically after $\approx 10$ $\mu$s. Calculation time is typically 3 days on a 6 cores of an Intel Xeon 3.0 GHz machine. Fig. 5 presents a typical evolution of the boundary currents. We observe that a quasi-converged state is obtained about 10 $\mu$s after discharge ignition.

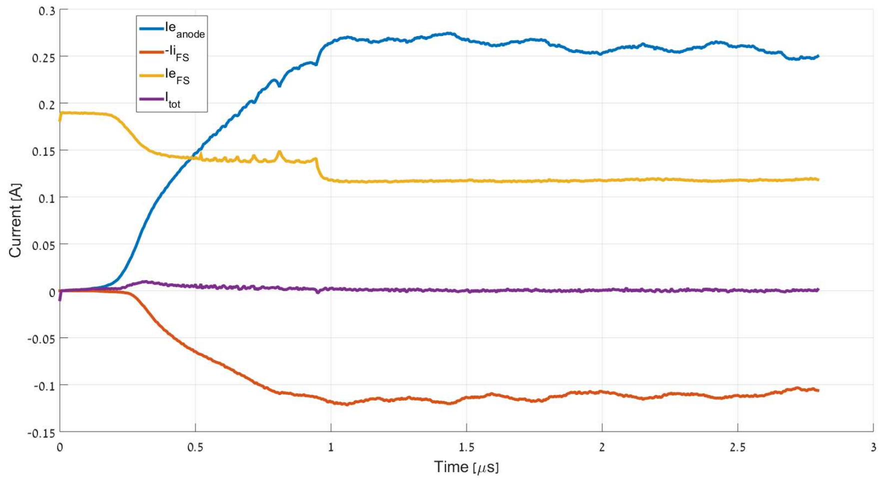


**Figure 5. Boundary currents during the ignition process, $t$=0 is the moment of electron injection. $I_e$ anode is the electron current to the anode, $I_{i,FS}$ and $I_{e,FS}$ are the ion and electron currents to the exit plane respectively, and $I_{tot}$ is the total axial current to the boundaries including the walls. Discharge parameters $\dot{m}$ = 0.4 mg/s, $U_d$ = 85 V, $I_{coil}$=0.5 A**

The parametric results of the simulated thruster can be obtained by considering the average ion velocity $\bar{v}_{i,ex}$ and ion current $I_{i,ex}$ at the channel exit. Using these parameters the thrust is computed by:

$$T = [(M/e)I_{i,ex}]\,\bar{v}_{i,ex}, \tag{1}$$

where $M$ is the xenon ion mass and $e$ the unit charge. Using the fact that the discharge current $I_d \approx I_{e,anode}$, the thruster anode efficiency $\eta_a$ can be calculated as:

$$\eta_a = \frac{[(M/e)I_{i,ex}]^2\,\bar{v}_{i,ex}^2}{2\dot{m}I_{e,anode}U_d}. \tag{2}$$

The thruster specific impulse, a measure of the ion exhaust velocity, is calculated by:

$$I_{sp} = \frac{T}{\dot{m}g_0}. \tag{3}$$

Table 2 presents the thruster global parameters as obtained by experimental measurements and channel simulation. These represent the best low power experimental results so far.[6]

**Table 2. NCHT parametric results.**

| Case #, | $\dot{m}$, mg/s | $U_d$, $V$ | $I_d$, A | $I_{i,ex}$, A | T, mN | $P_d$, W | $I_{sp}$, s | $\eta_a$, % |
|---|---|---|---|---|---|---|---|---|
| Exp. | 0.38 | 100 | 0.20 | 0.10 | 1.0 | 20 | 270 | 6.6 |
| Sim. | 0.38 | 100 | 0.14 | 0.075 | 0.83 | 14 | 282 | 8.2 |

## B. Spatial analysis of thruster discharge

The computed 2D spatial distribution of the electric potential $\phi$ is shown in Fig. 6. Several features are noticeable. The potential drop becomes asymmetric near anode and there are extended sheaths surrounding the metal walls that become thinner closer to the exit plane. More features can be analyzed by radially averaged 1D results, along the channel, shown in Fig. 7. The potential drop within the channel can be divided between 2 different zones, near the anode and near the exit plane. Similar acceleration layers or sheaths are known to occur in the thruster with anode layer (TAL).[15] Inside the sheath a balance exists between the electron diffusion current towards the anode that is driven by the temperature gradient and the electron diffusion current in the anode direction driven by the potential gradient. However, the exit plane sheath is assumed to be an artifact induced by the fixed potential boundary there (see Section III).

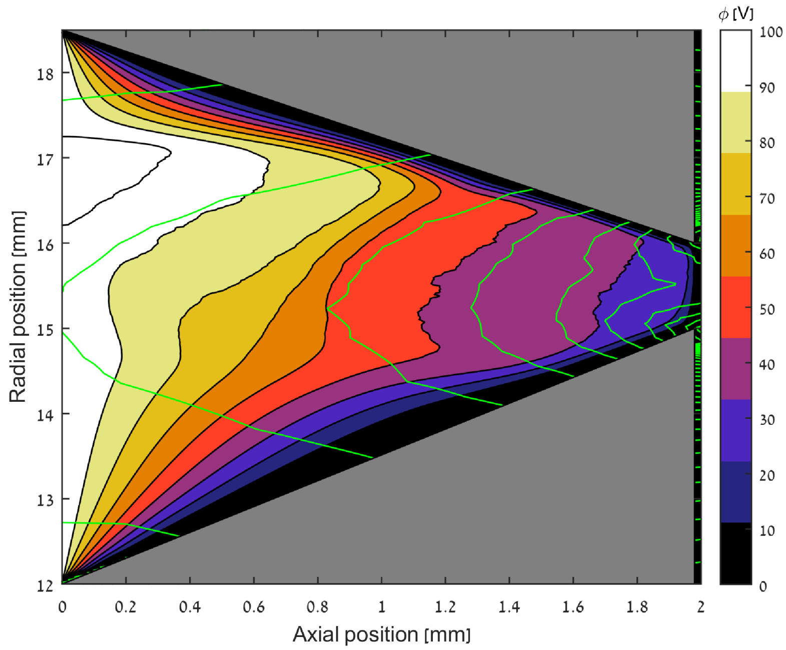


**Figure 6. Spatial distribution of electric potential contours. Magnetic field lines are shown green.**

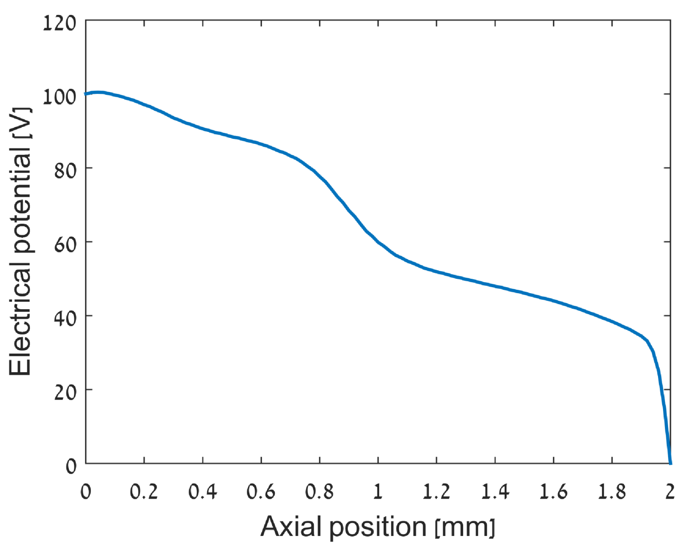


**Figure 7. 1D radially averaged electric potential along the channel.**

The ion density $n_i$ spatial distribution is shown in Fig. 8. We observe that the plasma $n_i \approx n_e \approx n$ covers a substantial part of the channel, with two distinct high density regions. The contact area of the plasma with the anode is larger than the cross sectional area of the exit plane. Since the plasma density is this part of the channel is low it effectively translates to an increase in resistance there. Therefore, larger anode area reduces the contact resistance, leading to lower potential drop in the anode sheath and to lower power losses by energetic electrons on the anode.

The ionization rate is calculated in each cell according to Eq. 4:

$$w_i \,|_{i,j} = [n_g n_e \sigma_i(\bar{v}_e)\bar{v}_e]_{i,j} \,. \tag{4}$$

where $n_g$ and $n_e$ are the number density of neutrals and electrons, respectively, $\bar{v}_e$ is the cell averaged electron velocity and $\sigma_i$ is the ionization cross section. The resulting map is shown in Fig. 9. We observe two distinct ion generation regions, one near the middle of the channel and one near the exit.

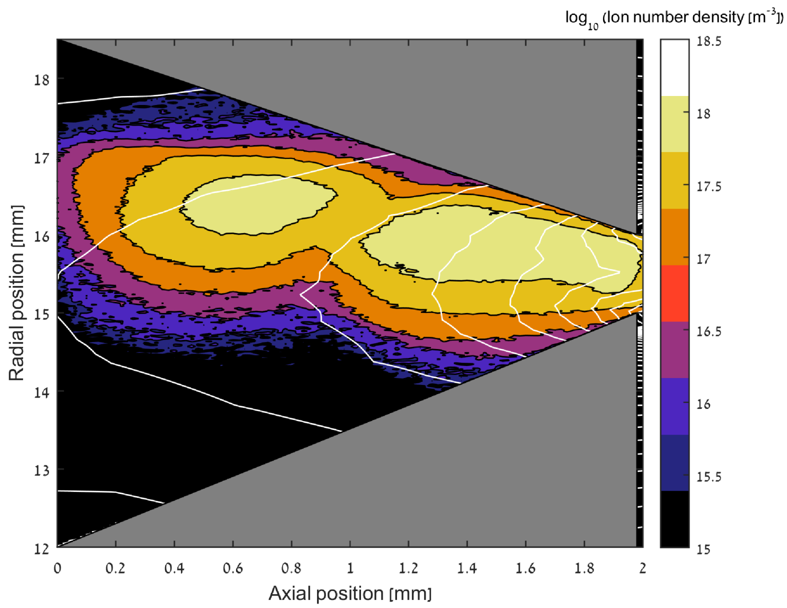


**Figure 8. Spatial distribution of plasma density contours. Magnetic field lines are shown white.**

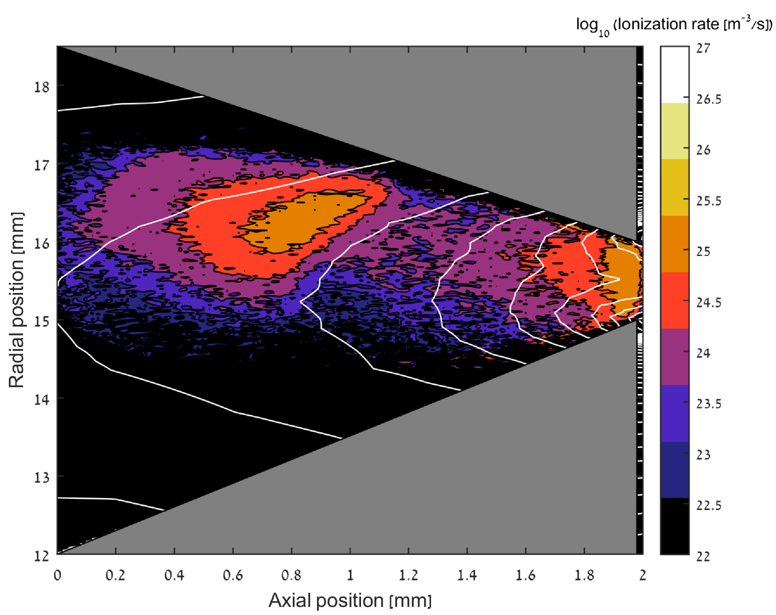


**Figure 9. Spatial distribution of ionization rate contours, $m^{-3}s^{-1}$. Magnetic field lines are shown white.**

The ion current distribution is shown in Fig. 10. Here we observe that most of the ion current is directed axially to produce thrust. However, up to 25 % of the ion current produced is lost to the walls, as shown in 11, which is higher than in classical HTs $\sim 10$ %. This result is not surprising given the fact the channel walls in the NCHT are much closer to the discharge. Notwithstanding, ion currents to the walls in the NCHT are less harmful (produce less erosion) than in conventional HTs due to the lower discharge voltage. By analyzing the ion macro-particles incident on the channel walls, the ion energy distribution function (IEDF) can be reconstructed. The mean ion energy obtained is $E_i < 50$ eV.

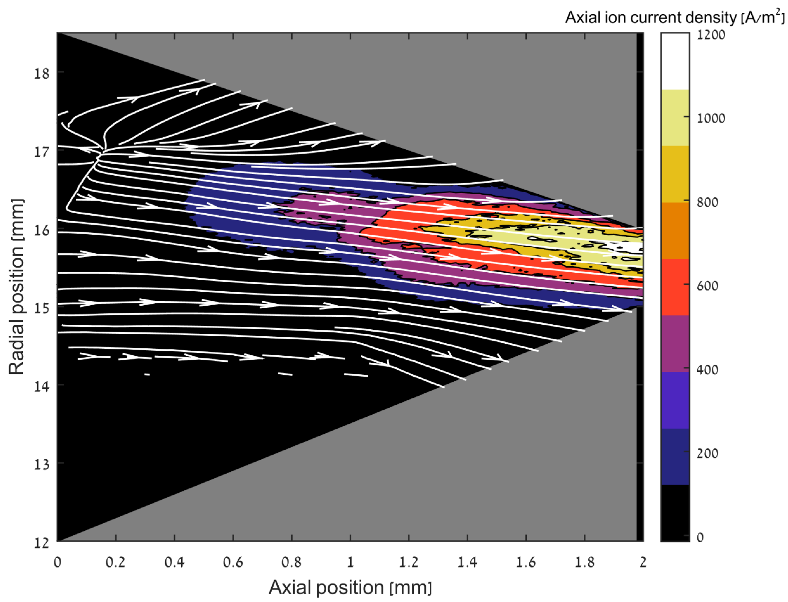


**Figure 10. Spatial distribution of ion current density contours. White lines are ion trajectories.**

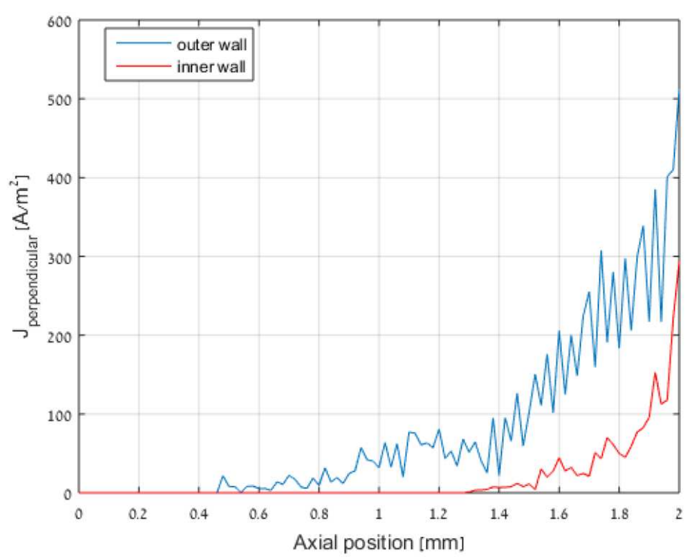


**Figure 11. Ion current density normal to the walls along the channel.**

Figure 12 shows radially averaged 1D discharge parameters along the channel, including: ion current density, electron kinetic energy, ion density and electric field. The ion axial current density is monotonically increasing towards the thruster exit. The maximum electron kinetic energy is obtained near the thruster exit with a secondary hot electron region upstream, both correspond to the two main ionization regions discussed earlier. The drop in the electron kinetic energy, which is caused by the energy losses associated with high degree of ionization, corresponds to the increase in the ion number density observed in these two distinct regions. The axial electric field has a peak near this zone close to the middle of the channel.

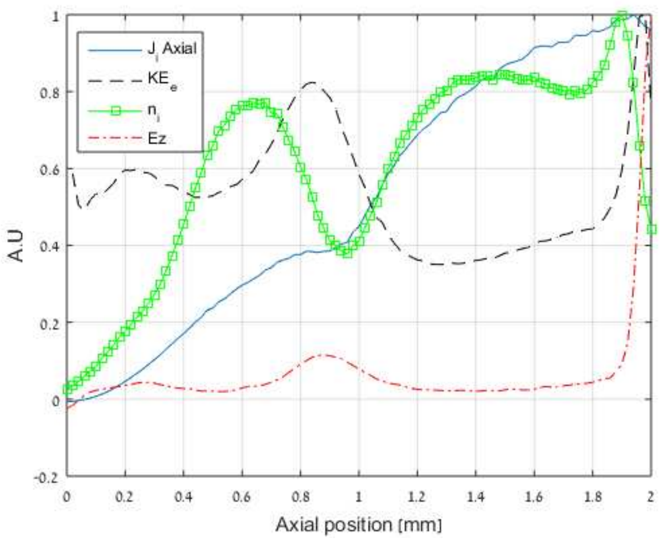


**Figure 12. Radially averaged and normalized plasma parameters along the axial direction.**

Comparison of experimental and simulation IEDF at the thruster exit plane is presented in Fig. 13. We observe that the computed IEDF has two distinct populations, a relatively narrow beam like population with $E_i \approx 55$ eV, that is over imposed on a background population. Although the beam like structure is not apparent in the experimental results, there is a good agreement with respect to the background population. The ion beam part of the simulations IEDF is produced by the sheath like structure near the thruster exit plane. The beam is an artifact of the imposed potential at the channel exit. Therefore, we can conclude that in reality the potential fall is gradual in the plume outside the thruster.

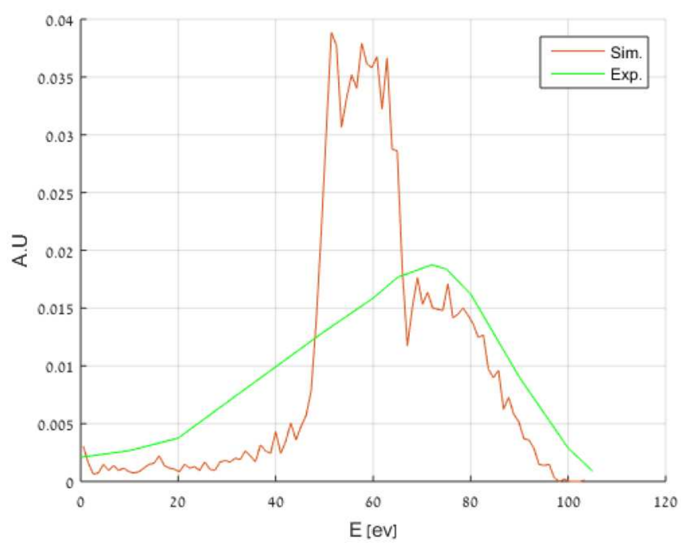


**Figure 13. Computed IEDF at the exit plane and measured IEDF.[6]**

Being fully kinetic, the simulation provides the velocity distribution of electron macro-particle species. Therefore, the Hall parameter can be calculated directly as a ratio between azimuthal and axial electron velocity components:

$$\Omega_e|_{i,j} = \left|\frac{\bar{v}_{e,\theta}}{\bar{v}_{e,z}}\right|_{i,j}, \tag{5}$$

where the indices are the coordinates of a specific cell. The calculation is performed in each cell by averaging the velocity components of all the macro-particles in that cell. In the classical description the electron perpendicular motion is only due to electron-neutral collisions, leading to:

$$\frac{v_{e,\theta}}{v_{e\perp}} \approx \omega_{ec}\tau_{e,tot} = \Omega_{e,class}, \tag{6}$$

where $\omega_{ec} = \frac{eB}{m_e}$ is the electron cyclotron frequency and $\tau_{e,tot} = \frac{1}{n_g\langle\sigma_{e,tot}v_e\rangle}$ is the electron-neutral momentum transfer collisional time, $m_e$ is the electron mass. Therefore the classical Hall parameter is:

$$\Omega_{e,class} \approx \frac{eB_r}{m_e n_g \langle\sigma_{e,tot}v_e\rangle}, \tag{7}$$

where $B_r$ is the magnitude of the radial component of the magnetic field. The axial distribution of the actual Hall parameter $\Omega_e$, calculated using Eq. 5, and the classical Hall parameter $\Omega_{e,class}$, calculated using Eq. 7, are shown in Fig. 14. We observe that along most of the channel $\Omega_e \sim 16$ - 32. However a limited zone exists around 0.8 mm where classical values are restored. This narrow zone delimits the region where magnetic field lines no longer intersect the anode.

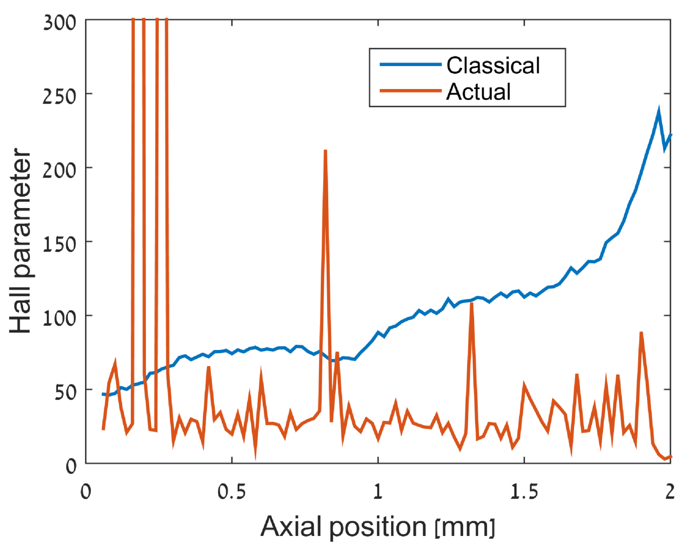


**Figure 14. Radially averaged distribution of the Hall parameter. Both classical and actual Hall parameters are shown.**

# V. Conclusion

The discharge in the NCHT channel was analyzed using a fully kinetic 2D PIC simulation. The small size of the NCHT and the application of parallel computation allows relatively fast first principle calculation of thruster performance. The simulation allows the characterization of the spatial variation of plasma parameters where experimental investigation is virtually impossible. The simulation was validated against experimental parametric results for mass flow rate of 0.38 mg/s. It was found that the NCHT current leakage towards the anode is substantial, near Bohm's value. However, the formation of a magnetized near anode sheath enables significant ionization within the channel. The simulation results are effected by the imposition of a fixed potential boundary at the channel exit. More accurate results are expected once the near field plume region will be included in the simulation domain.

## References

[1]Goebel D M and Katz I 2008 *Fundamentals of Electric Propulsion* (New York: Wiley)

[2]Shagayda A A and Gorshkov O A 2013 Hall-Thruster Scaling Laws *J. Propul. Power* **29** pp 466–474

[3]Ashkenazy J, Shitrit S and Appelbaum G 2005 *29th International Electric Propulsion Conf. (Princeton University, NJ)* paper 2005-080

[4]Raitses Y and Ashkenazy J 1996 *XVIIth International Symposium on Discharges and Electrical Insulation in Vacuum (Berkeley, CA)* **1** pp 492–496

[5]Hofer R R, Peterson P Y, Gallimore A D and Jankovsky R S 2001 *27th International Electric Propulsion Conf. (Pasadena, CA)* paper 2001-036

[6]Kronhaus I and Linossier A 2018 *Plasma Sources Sci. Technol.* **27** 124005

[7]Kronhaus I, Kapulkin A, Guelman N and Natan B 2012 *Plasma Sources Sci. Technol.* **21** 035005

[8]Verboncoeur J P, Langdon A B and Gladd N T 1995 *Comp. Phys. Comm.* **87** 199–211

[9]Meeker D C 2010 *Finite Element Method Magnetic* http://www.femm.info

[10]Birdsall C K and Langdon A B 1991 *Plasma Physics via Computer Simulation* (Adam Hilger: Bristol, UK)

[11]Hockney R W and Eastwood J W 1988 *Computer Simulation Using Particles* (Adam Hilger: Bristol)

[12]Dagum L and Ramesh M 1998 *IEEE Comp. Sci. Eng.* **5** pp. 46–55

[13]Seward J and Nethercote N and Weidendorfer J and the Valgrind Development Team 2008 *Valgrind 3.3 - Advanced Debugging and Profiling for GNU/Linux Applications* (Network Theory Ltd: Bristol, UK)

[14]Szabo J 2001 *DPhil Thesis* Massachusetts Institute of Technology

[15]Zhurin V V and Kaufman H R and Robinson R S 1999 *Plasma Sources Sci. Tech.* **8** 1–20